

TRIPLE NONLINEAR HYPERBOLIC PID WITH STATIC FRICTION COMPENSATION FOR PRECISE POSITIONING OF A SERVO PNEUMATIC ACTUATOR

KHAIRUN NAJMI KAMALUDIN¹, LOKMAN ABDULLAH^{1*},
SYED NAJIB SYED SALIM², ZAMBERI JAMALUDIN¹, NUR AIDAWATY RAFAN¹,
MOHD FUA'AD RAHMAT³ AND RPRAKASH RAMANATHAN¹

¹Faculty of Manufacturing Engineering, Universiti Teknikal Malaysia Melaka,
Hang Tuah Jaya, 76100 Durian Tunggal, Melaka, Malaysia

²Faculty of Electrical and Electornic Engineering Technology, Kampus Teknologi,
Universiti Teknikal Malaysia Melaka, Hang Tuah Jaya, 76100 Durian Tunggal,
Melaka, Malaysia

³Department of Control and Mechatronic Engineering (CMED), Faculty of Electrical
Engineering, Universiti Teknologi Malaysia Johor Bahru, 81310, Malaysia

*Corresponding author: lokman@utem.edu.my

(Received: 28 February 2023; Accepted: 10 May 2023; Published on-line: 4 July 2023)

ABSTRACT: Accurate and precise positioning control is critical in designing a positioning servo pneumatic system. The internal friction force of the pneumatic is one of the disturbances that make it challenging to achieve accurate and precise positioning. Dynamic friction identification and modelling are usually very complex and computationally exhaustive. In addition, pneumatic actuators are nonlinear systems, and applying linear control to the system is a mismatch. This study proposes an enhanced triple nonlinear hyperbolic PID controller with static friction (T-NPID+ F_{SS}) feedback module. T-NPID is integrated with nonlinear hyperbolic functions at each PID gain, hence the name. The reference in designing the T-NPID is the Popov stability criterion. Meanwhile, static friction (comparatively more straightforward than dynamic friction) is identified by measuring the actuator's internal friction at various velocities and applying it to the static friction model. T-NPID+ F_{SS} is compared to a classical PID, a PID with static friction (PID+ F_{SS}), and T-NPID without the friction module. With the comparisons, the performance gains of each module are clear. While most previous research focuses on the sinusoidal wave tracking performance (measuring the maximum tracking error, MTE, and root mean square error, RMSE), the analysis in this research focuses on obtaining precise positioning; steady-state analysis is the primary measurement. However, transient response and integral of absolute error (IAE) analysis are also observed to ensure no significant drawback in the controller's performance. T-NPID+ F_{SS} achieved the best precise positioning control, with 88.46% improvement over PID, 71.15% over PID+ F_{SS} , and 59.46% over T-NPID. The final controller is also on par with T-NPID for transient responses compared to the base PID. Although the F_{SS} model caters to friction compensation, optimizing the F_{SS} parameter by applying artificial intelligence, such as Neural Networks (NN) and Genetic Algorithm (GA), will increase the friction modeling's accuracy, and improve the compensation.

ABSTRAK: Kawalan kedudukan tepat dan jitu adalah kritikal dalam mereka bentuk sistem pneumatik servo penentu. Daya geseran dalaman pneumatik merupakan salah satu gangguan yang menyukarkan bagi mencapai kedudukan yang tepat dan jitu. Penentuan dan pemodelan daya geseran dinamik kebiasaannya sangat kompleks dan melibatkan pengiraan menyeluruh. Tambahan, penggerak pneumatik adalah sistem tak linear, dan

menggunakan kawalan linear pada sistem adalah tidak sesuai. Kajian ini mencadangkan kawalan PID hiperbolik tiga fungsi tak linear yang dipertingkatkan dengan modul suapan-balik geseran statik (T-NPID+ F_{SS}). T-NPID diintegrasikan dengan tiga fungsi hiperbolik tidak linear pada setiap pekali PID, seperti namanya. T-NPID direka bentuk dengan kriteria kestabilan Popov. Manakala geseran statik (secara perbandingan lebih mudah daripada geseran dinamik) dikenal pasti dengan mengukur penggerak geseran dalaman pada pelbagai halaju dan menerapkannya pada model geseran statik. T-NPID+ F_{SS} dibandingkan dengan PID klasik, PID dengan geseran statik (PID+ F_{SS}) dan T-NPID tanpa modul geseran. Melalui perbandingan, prestasi peningkatan setiap modul adalah jelas. Walaupun kebanyakan kajian terdahulu memfokuskan pada prestasi penentuan gelombang sinusoidal (mengukur ralat penentuan maksimum, MTE dan ralat purata kuasa dua, RMSE), analisis kajian ini memberi tumpuan kepada mendapatkan kedudukan yang tepat; oleh itu, analisis keadaan akhir adalah ukuran utama. Namun, tindak balas sementara dan analisis kamiran ralat mutlak (IAE) juga diperhatikan bagi memastikan tiada kekurangan ketara dalam prestasi kawalan. T-NPID+ F_{SS} mencapai kawalan penentuan kedudukan tepat terbaik, dengan peningkatan 88.46% berbanding PID, 71.15% berbanding PID+ F_{SS} dan 59.26% berbanding T-NPID. Kawalan akhir yang dicadangkan juga adalah setanding dengan T-NPID bagi respons sementara berbanding PID asas. Walaupun model F_{SS} memenuhi pampasan geseran, mengoptimumkan parameter F_{SS} dengan menggunakan kecerdasan buatan (*artificial intelligence*, AI) seperti *Neural Networks*, NN dan *Genetic Algorithms*, GA akan meningkatkan ketepatan dan pampasan pemodelan geseran.

KEYWORDS: *servo pneumatic actuator; nonlinear control; PID controller; steady-state error; transient response; static friction*

1. INTRODUCTION

Many industrial applications such as those requiring manipulators, riveting machines, automobiles, pick-and-place devices, and others have made extensive use of pneumatic actuators. This is because pneumatic systems have a variety of benefits, including ease of maintenance, lower cost, low heat under steady load and many others [1-3]. The pneumatic actuator continues to garner ever more research interest as a result of these benefits. However, achieving the performance of great precision and accuracy yields obstacles. Nonlinear pneumatic actuators present challenges in the forms of control field with disturbances such as wide dead zones, air compression nonlinearity, low damping, and frictional forces [4]. The internal friction force is agreed to be one of the critical disturbances in an actuator that affects the performance needed to achieve precise positioning and trajectory tracking in a servo system [5-6]. In a pneumatic actuator, friction occurs between the seal and the internal cylinder wall [5,7]. According to a review by [8], friction force compensation is mainly compensated by scholars compared to other disturbances such as air pressure and dead zone, which shows that it is a major disturbance in this field.

The PID controller is a linear control scheme and modifying a PID controller by integrating other elements, such as fuzzy and nonlinear mathematical functions, ultimately changes the controller's characteristics into a nonlinear control scheme. It is still desirable to enhance and improve the classical PID controller since it is the most widely used in the industry [9-10]. Integrating a PID together with other industrial automation control such as Programmable Logic Control (PLC), SCADA and a few others is a proven workable solution [11-12]. Nonlinear controllers for servo pneumatic systems usually adapt sliding mode controllers (SMC) [13-15], as well as a few other controllers such as model reference adaptive controller (MRAC) [16], fuzzy logic controllers (FLC) [17] and neural network (NN) controller [18]. Nonlinear controllers are commonly complex and are less applied in the industrial field.

An example of a controller that adapts both nonlinear controls with a friction compensation is an SMC with generalized Maxwell Slip (GMS) dynamic friction as explored by [19], whereby the author adapts both dynamic and static friction. The GMS model is applied during near zero velocity while static friction is implemented during velocity. The system reduces tracking errors compared to the Stribeck friction model. However, obtaining the zero-velocity hysteresis model is complex, as other models need to be applied. Another research adapting multiple surface SMC (MSSMC) with a friction model is by [20]. A dynamic LuGre model is employed for the dynamic friction compensation. The MSSMC were compared with and without the friction observer proving that the observer yields a lower tracking error. The derivation of MSSMC is complex and challenging due to the inputs required other than position, such as velocity and pressure. A study by [21] presented a dynamic adaptive backstepping SMC (DAB-SMC) with LuGre friction model compensation. The controller with friction compensation resulted in up to 15% in root mean square error (RMSE) in step positioning and sine-wave tracking. No nonlinear-PID (N-PID) based controllers have been successfully developed adapting friction compensating modules. Some examples of N-PID, such as [22] developed an enhanced self-regulating nonlinear PID (SN-PID) in which the nonlinear function's variables were designed to be adaptive using a self-regulating function. The same author also developed a multi-rate nonlinear PID (MN-PID), where the nonlinear function varies with the control of fuzzy logic and the disturbance compensated is the valve dead zone. The difference before and after adapting the module compensator was not calculated so the improvement rate was not concluded. [23] proposed a nonlinear PI (N-PI) controller without any add-on disturbance compensating module. The research focused on overshoot reduction, validating a few N-PI controllers against the classical PI controller. However, the precise positioning or steady-state results were also not presented.

Owing to the recent research gap in advances for N-PID, this research attempts to explore and analyze a new strategy of N-PID in combination with the friction disturbance compensator. T-NPID was previously developed to improve the performance of a classical linear PID enhancing the sinewave trajectory tracking for precise positioning performance of an XY table ball-screw system and step response of a servo pneumatic plant [24-25]. T-NPID would be a better match to the nonlinear characteristics of the servo pneumatic plant as explained by [4-5]. The stability of the controller is validated via Popov stability criterion. Finally, the static friction compensation module will enhance the T-NPID by compensating for the internal friction, therefore increasing the final steady-state positioning performance of the pneumatic system.

2. METHODOLOGY

2.1 Experimental Plant Configuration and Plant Modeling

The experimental plant configuration and equipment model used in the plant are presented in Fig. 1 and Table 1. The input and output signals are connected to the main electrical junction box which is then connected to the data acquisition (DAQ) module, allowing for two-way communication with the personal computer (PC). The human-machine interface utilized in this research is Matlab with a Simulink environment.

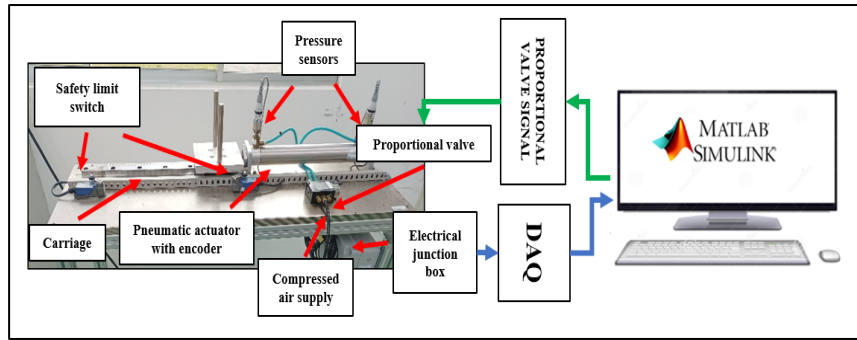


Fig. 1: Experimental plant setup and configuration.

Table 1: Equipment utilized for the experimental plant

Equipment	Model number	Specification
Proportional valve	Enfield LS-V15s	5/3 port, 0-10 Volts
Pneumatic actuator with integrated position encoder	Enfield ACTB-200-S10200	Double acting, 12 inch/ 304.80 mm stroke length
Pressure sensor	Gems Sensor 1200SGG	0 to 10 volts, 0-150 PSI
Safety limit switch	Tezuo AZ8104	Contact on
DAQ Box	National Instrument PCI-6221	37 Pin PCI
Matlab / SIMULINK	Version 2016b	N/A

In the control system field, modeling the experimental plant is the first predefined step before any other analysis or design is executed as agreed upon and performed by [26-27]. Modeling of the plant is performed using the system identification toolbox in Matlab. A predefined multi-sinewave signal in Volts is inserted into the experimental system in an open loop setup, and the response (in millimeters or voltage) of the system is recorded as explained by [28-29]. A pneumatic actuator is a nonlinear system; therefore, modeling of the plant is expressed in the state space matrix model. Linearization of the state space to a transfer function expression is also preferred for analysis simplification in the Matlab editor environment, such as gain margin, phase margin, and Nyquist stability analysis. The continuous state space matrix modeling is presented in Eq. (1) to Eq. (4). Linearization to the transfer function yields a third-order model as expressed in Eq. (5). The best-fit percentage obtained via system identification is 91.99%. Therefore, the model is valid for the analysis and design [28,30-31]. The block diagram presents the system's transfer function as a 'G' plant, as shown in Fig. 2.

$$A = \begin{bmatrix} -0.2921 & -0.02056 & -0.000085 \\ 1 & 0 & 0 \\ 0 & 1 & 0 \end{bmatrix} B = \begin{bmatrix} 1 \\ 0 \\ 0 \end{bmatrix} \quad (1)$$

$$C = [0.03468 \quad 0.1468 \quad -0.002041] D = [0] \quad (2)$$

$$\dot{x} = Ax + Bu \quad (3)$$

$$y = Cx + Du \quad (4)$$

where A are the state vectors, B is the measured output, C are the measured input and D is noise.

$$G(s) = \frac{0.03468s^2 + 0.1468s - 0.002041}{s^3 + 0.2921s^2 + 0.02056s + 0.000085} \quad (5)$$

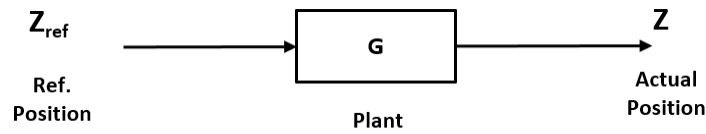


Fig. 2: Transfer function ‘G’ in a schematic block diagram.

2.2 Static Friction Identification and Modeling

Identifying the system’s internal friction force is critical in order to compensate for the known disturbance. Identification of the static friction (also generally known as the sliding regime) requires the friction to be determined in the presence of velocity. Figure 3 presents the general friction force characteristics of velocity, with the presence of Stribeck and viscous friction effects [32]. The mathematical expression of the static friction, F_{SS} , is presented by Eq. (6) [19].

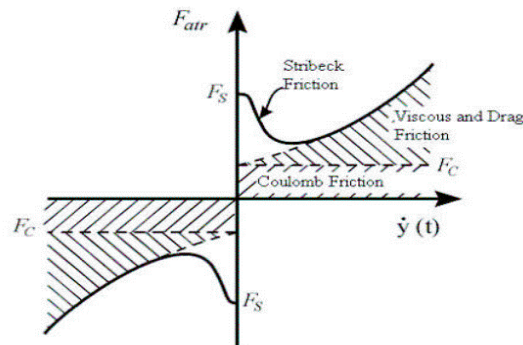


Fig. 3: Static friction model [7].

$$F_{SS}(v) = \text{sgn}(v) \cdot \left[F_c + (F_s - F_c) e^{-\left(\frac{v}{v_s}\right)^2} \right] + F_v \cdot v \quad (6)$$

where v , F_c , F_s , V_s and F_v are illustrated as velocity, Coulomb friction, static friction, Stribeck velocity and viscous friction, respectively.

To obtain each of the parameters expressed in Eq. (6) multiple voltages are applied to the valve of the system in an open loop configuration to actuate the pneumatic actuator to move in various constant velocities [32-33]. The pressure difference between the two pneumatic actuator chambers is recorded at each constant velocity. The difference in the pressure is converted to force by the equation $f = p \times a$, where f is the friction force, a is the effective area of the internal pneumatic piston, and p is the known pressure measured by the pressure sensor. The actuator’s obtained friction force versus velocity is shown in Fig. 4.

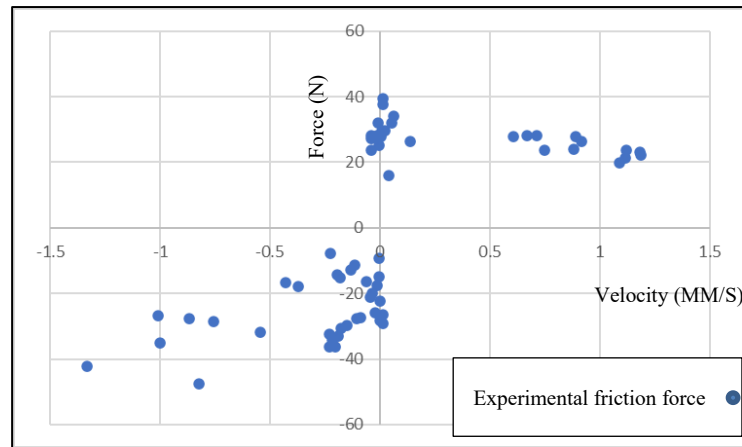


Fig. 4: Experimental plot for velocity versus friction force.

A model of static friction is compared to the force versus velocity plot and optimized by a best-fit curve. A comparison of the model overlapped with the actual force from Fig. 4 is presented in Fig. 5 (a) and the final model applied as the F_{SS} model is shown in Fig. 5 (b). Table 2 displays the obtained static friction parameters in Eq. (6).

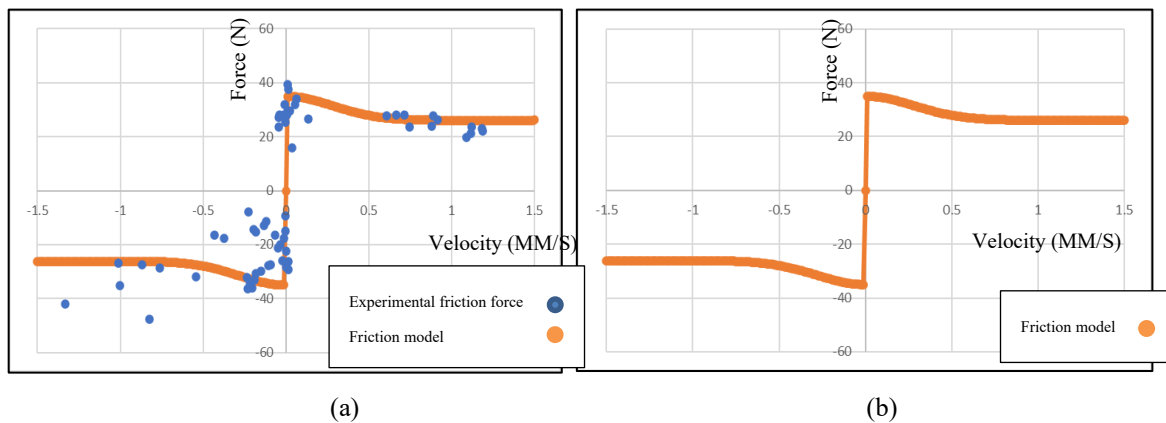


Fig. 5: (a) Comparison of the actual friction force and friction model; (b) applied friction model.

Table 2: Static friction parameter value

Static friction parameter	Parameter value
Coulomb friction, F_c (Newton)	26
Stribeck friction, F_s (Newton)	35
Stribeck velocity, V_s (mm/s)	0.4
Viscous friction, F_v (Newton-second / mm)	0.1

2.3 Validation of Friction Model with System Modeling

The static friction model is a feedback block to the transfer function, as presented in Fig. 6 [33]. Since the output of the transfer function block G is position (in mm), a derivative function is required to convert the displacement velocity of the actuator during motion as an input to the friction model, F_{SS} . A gain is used to convert the force value (in Newton) to voltage (volts). The procedure is conducted in a closed-loop system response by applying different known forces to the system multiple times. The counteract voltage by the controller is recorded. The gain obtained is, $K_f = -1/2020.20$ volt/Newton, as presented in Table 3. In

simple terms, the K_f gain translates to the system requiring 0.000495 volts to overcome 1 Newton of force.

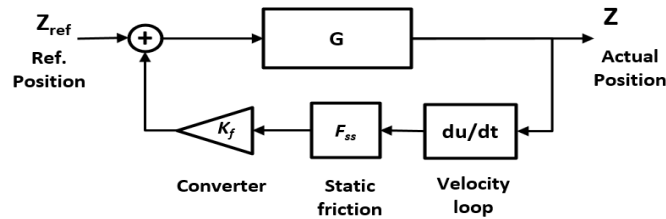


Fig. 6: Modeling of the friction force with the servo pneumatic plant.

Table 3: Newton to voltage converter gain, K_f

Gain type	Parameter value
K_f	-1/2020.20

Validation of the transfer function with the friction model is conducted by comparing the new plant and friction model in a simulation environment with the experimental response [34]. The same sinusoidal input performed during the system identification process is supplied to the new transfer function with the static friction model, and the output response data is captured. In order to observe the accuracy of modeling, the best-fit percentage is recalculated based on Eq. 7 [35-36] using the same equation applied by the Matlab system identification toolbox explained in Section 2.1. If the best-fit percentage drops below a predefined threshold of 90% accuracy, adjustment of the transfer function of plant ‘G’ will be required [32][37]. Figure 7 shows the estimation model and experimental data for the best-fit percentage calculation.

$$Best\ fit\ percentage = \left(1 - \frac{\sum |\hat{y}_{estimate} - y_{experimental}|}{\sum |y_{experimental} - y_{mean}|} \right) \times 100\% \quad (7)$$

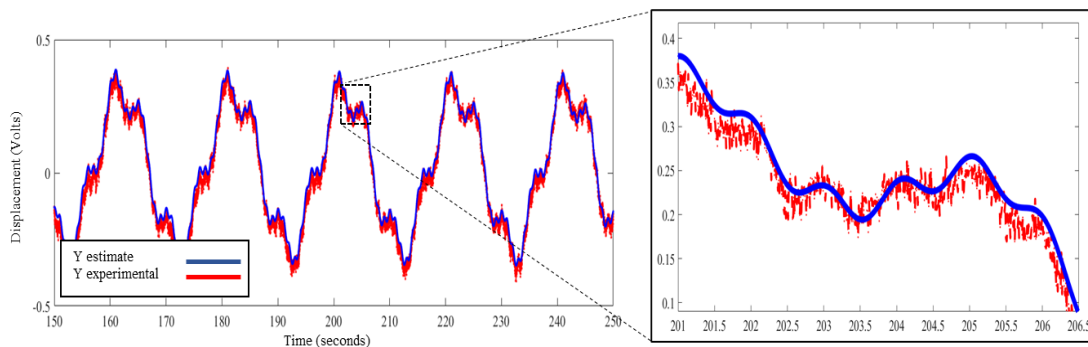


Fig. 7: Comparison of experimental data and model with friction data.

The best-fit percentage after including the static friction in the model is 91.373% which has decreased by 0.617% based on the initial system identification process. Although there is a reduction of modeling accuracy, the threshold of 90% is still in place; therefore, adjusting the transfer function is unnecessary in this case.

2.4 Design of PID Controller

Figure 8 presents a general PID block diagram for the plant. In this research, plant ‘G’

is modeled with static friction ($G+F_{ss}$). The process flow related to tuning the PID controller gains follows the previous procedure performed by [25]. Table 4 tabulates the gain parameters obtained for the PID controller.

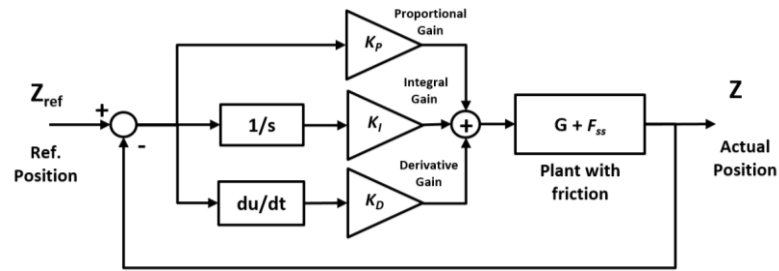


Fig. 8: General PID controller with plant block diagram.

Table 4: PID controller parameter

Gain type	Gain values
Proportional gain, K_P	10
Integral gain, K_I	0.1925
Derivative gain, K_D	0.35

2.5 Stability of PID Controller

Once the PID parameters are obtained, the Nyquist stability theorem is applied to the PID controller. An open loop configuration is observed in a Nyquist plot. Referring to Fig. 9, it is observed that the Nyquist plot does not encircle at -1 on the real axis, thus it is concluded that the system is stable.

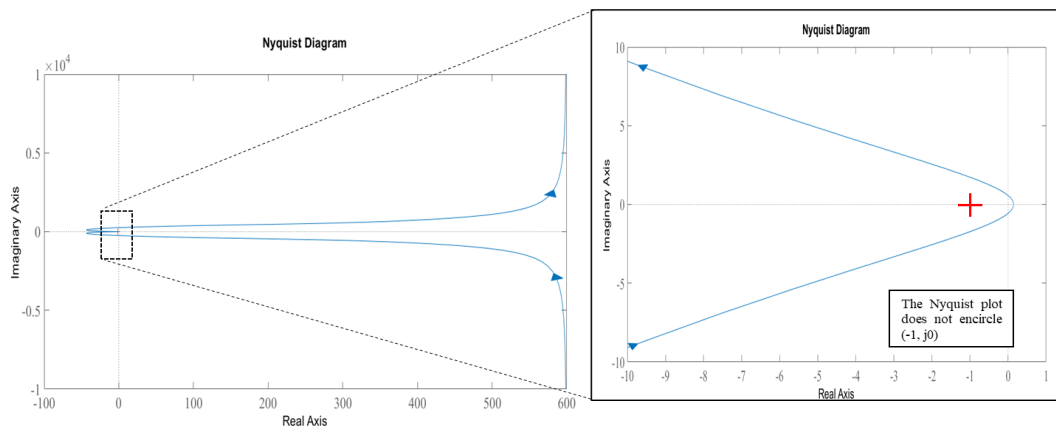


Fig. 9: (a) Nyquist plot for plant with PID controller; (b) close-up of Nyquist plot.

2.6 Design of the Triple Hyperbolic T-NPID Controller

Figure 10 presents the T-NPID block diagram. Three individual nonlinear hyperbolic functions are cascaded at each PID gain. The nonlinear hyperbolic functions are as presented in Eq. (8) to Eq. (10). Each nonlinear function will adapt accordingly to the error produced, multiplying the error exponentially if the error increases until the limit of predetermined maximum error, e_{Max} . Since there are three individual nonlinear functions, the errors are multiplied individually by the PID gains, adding flexibility to each gain of the PID.

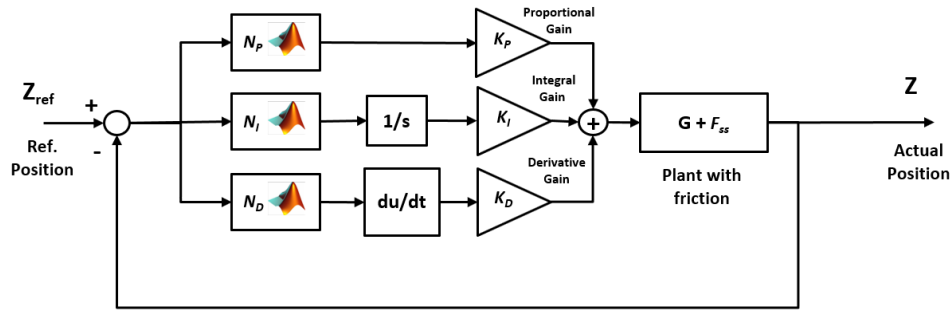


Fig. 10: Block diagram of a plant with friction model and T-NPID controller.

The errors are processed at each of the nonlinear function blocks before the nonlinear functions are multiplied by the error [24]. If the absolute error is smaller than or equal to e_{Max} , then the error is used by the nonlinear function. If the absolute error is larger than e_{Max} , then e_{Max} is multiplied by the signum of error and applied to the nonlinear function. The function written in each function block is as follows:

```

if
abs(error) <= e_Max,
error = error;
else
e = (e_Max) * sign(e);
end

```

$$K_p(e) = 1 + f \times [1 - \text{sech}(g \times e_p)] \quad (8)$$

$$K_i(e) = 1 \div [p + q \times (1 - \text{sech}(r \times e_l))] \quad (9)$$

$$K_d(e) = 1 + a \times [1 - \text{sech}(b \times e_d)] \quad (10)$$

The constants in Eq. (8) to Eq. (10) are tuned as per previous research [25]. Each parameter is tuned to achieve the best steady-state or actual positioning results. In addition, further tuning of the parameter was also performed to improve the transient response of the system. All the constants or parameter values are tabulated in Table 5.

Table 5: Nonlinear function parameter

Paramater	Value
f	1.65
g	30.1
e_p	0.095
p	34
q	24
r	10
e_l	0.35
a	1.9
b	1.75
e_d	0.25

Popov stability criterion is utilized in order to check the stability of the system with T-NPID controller. This criterion is a guideline so that the nonlinear gains operate within an allowable region of the controller and plant [38]. A reduced transfer function of the plant is applied for the analysis simplification [39]. In this research, three Popov plots from the criterion are developed as three nonlinear functions are applied at each PID gains. For each Popov plot, different equations are applied. The individual PID components Popov equations from Eq. (11) to Eq. (16) are summarized from the detailed analysis of [40].

The nonlinear P component of the Popov plot expression is in Eq. (11) and Eq. (12):

$$\mathcal{Re}W(j\omega) = \frac{k(-K_P \cdot \omega^2 + j \cdot K_P)}{[d^2 \cdot \omega^2 + (j - \omega^2)^2]} \quad (11)$$

$$\omega \mathcal{Im}W(j\omega) = \frac{-k(d \cdot K_P \cdot \omega^2)}{[d^2 \cdot \omega^2 + (j - \omega^2)^2]} \quad (12)$$

The nonlinear I component of the Popov plot expression is in Eq. (13) and Eq. (14):

$$\mathcal{Re}W(j\omega) = \frac{k(d \cdot K_I)}{[d^2 \cdot \omega^2 + (j - \omega^2)^2]} \quad (13)$$

$$\omega \mathcal{Im}W(j\omega) = \frac{-k(-K_I \cdot \omega^2 + j \cdot K_I)}{[d^2 \cdot \omega^2 + (j - \omega^2)^2]} \quad (14)$$

The nonlinear D component of the Popov plot expression is in Eq. (15) and Eq. (16):

$$\mathcal{Re}W(j\omega) = \frac{k(d \cdot K_D)}{[d^2 \cdot \omega^2 + (j - \omega^2)^2]} \quad (15)$$

$$\omega \mathcal{Im}W(j\omega) = \frac{-k(K_D \cdot \omega^4 - j \cdot K_D \cdot \omega^2)}{[d^2 \cdot \omega^2 + (j - \omega^2)^2]} \quad (16)$$

2.7 Design of the T-NPID with Static Friction Compensator (T-NPID+ F_{SS}) Controller

The final T-NPID+ F_{SS} controller is shown in Fig. 11. The friction compensator (within the box) is the same basic schematic configuration as the static friction modeled in Fig.6. The difference is the summing junction attached to the plant, where the T-NPID+ F_{SS} is subtracting the simulated friction, in other words, compensating for the friction. This configuration is in line with the general friction observer and compensator reviewed by [8]. For schematic simplifying, the friction compensator is combined as a simple block, F_{SS} , as shown in Fig. 12.

In experimental mode, the basic schematic is shown in Fig. 13. The modeled plant and friction in the simulation, as shown in the previous basic schematics, are changed to the proportional valve and the actuator position encoder. The output of the TNPID+ F_{SS} is connected to the plant's proportional valve, and the plant's output, the actual position (Z), is obtained from the actuator position encoder. Z is feedback for both friction compensation and a closed-loop controller system.

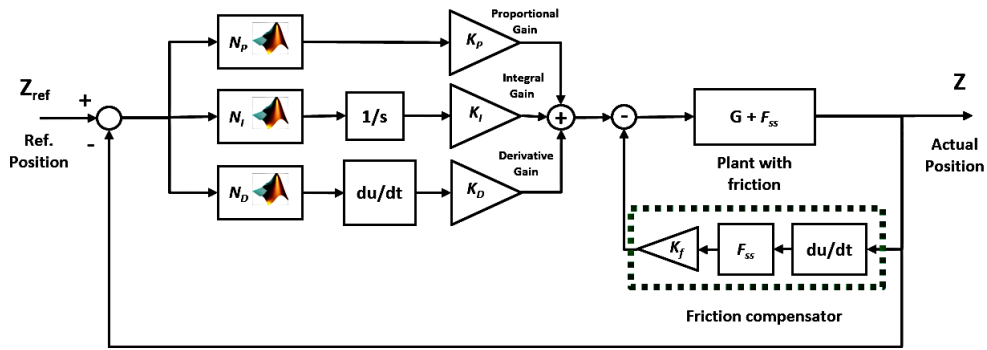


Fig. 11: The T-NPID+ F_{SS} controller scheme.

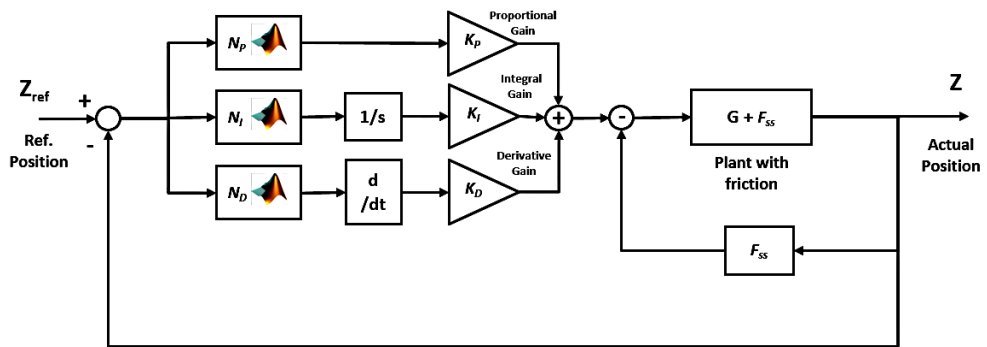


Fig. 12: Simplifying the friction compensator basic schematic.

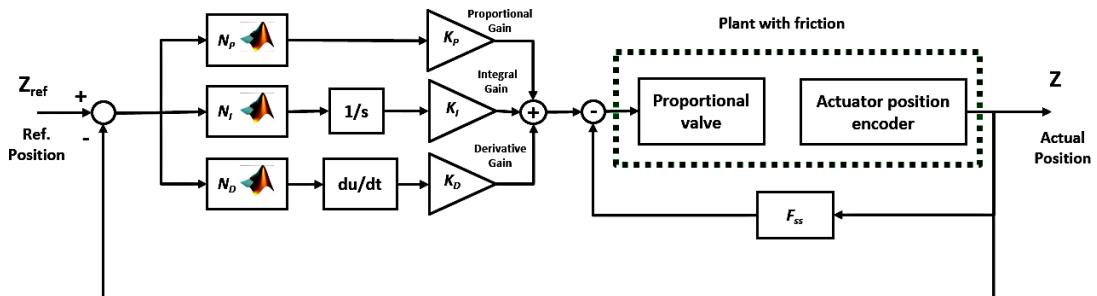


Fig. 13: The basic schematic in experimental mode T-NPID+ F_{SS} and servo pneumatic plant.

2.8 Stability of the Triple Hyperbolic T-NPID Controller

The Popov stability criterion application has been described in detail by [38]. The Popov plot for P, I, and D components are shown in Figs. 14, 15, and 16, respectively. Both the P and D controller Popov plot does not cross the real axis; therefore, the maximum allowable gain K is $(0, \infty)$. The real axis is the y-axis (imaginary axis) at 0, as shown in Fig 14. The closed loop nonlinear gain is always stable for the P and D components. The Popov plot crosses the real axis at $(-34.1202, 0)$ for the I component. To obtain the maximum allowable gain, Eq. (17) is applied; therefore, the $K_I(e)$ value must be between 0 and 0.0293 ($0 < K_I(e) < 0.0293$).

$$K(e_{Max}) = -\frac{1}{\text{Re}\omega(j\omega_0)} \quad (17)$$

From Eq. (8) to Eq. (10), the value of $K_P(e_{Max})$, $K_I(e_{Max})$, and $K_D(e_{Max})$ are obtained as 2.4616, 0.028, and 1.1683, respectively, based on the range of allowable nonlinear gain

and the best steady-state position obtained. These values are obtained after the determination of the hyperbolic algorithm parameters.

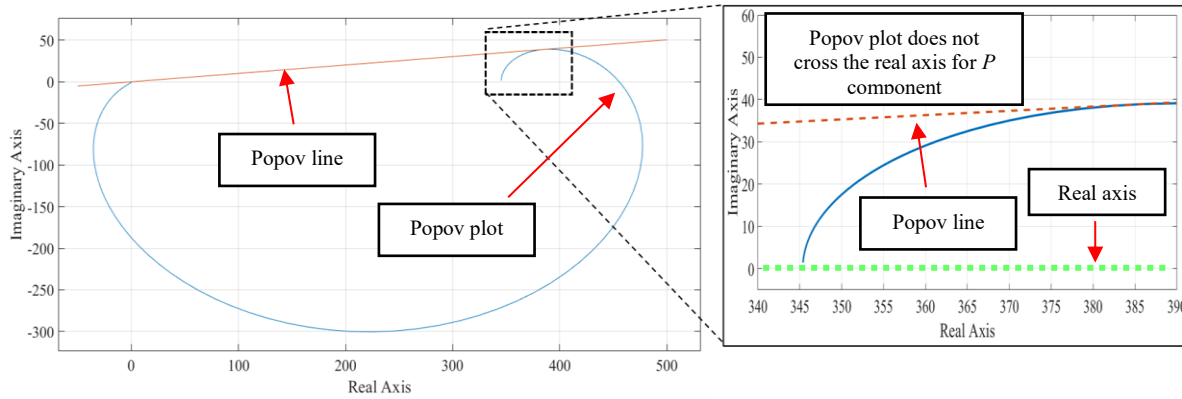


Fig. 14: The P component Popov plot.

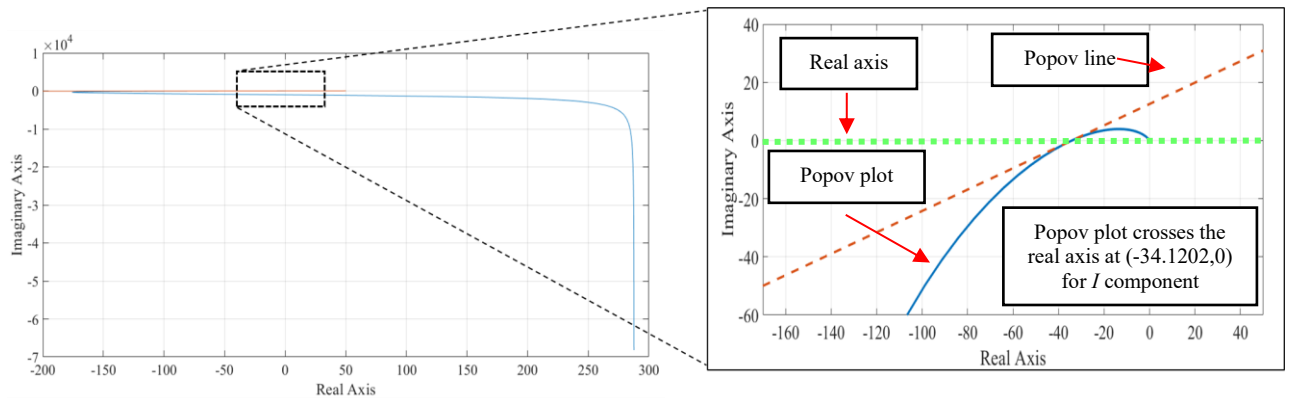


Fig. 15: The I component Popov plot.

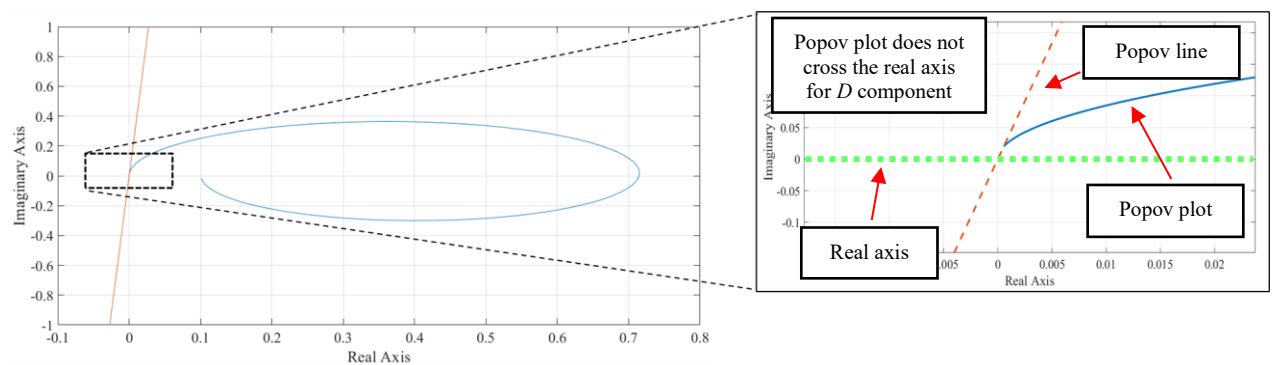


Fig. 16: The D component Popov plot.

Each method for designing the compensators has been presented in this section. Altogether three compensators were analyzed and compared to the typical PID controller. The first compensator is PID with the added friction force compensator, $PID+F_{SS}$. By adding F_{SS} only, the performance gains will be able to be analyzed and discussed. The next compensator is the T-NPID. T-NPID is anticipated to improve significantly even without friction compensation due to its system error-handling characteristic. The final compensator is T-NPID+ F_{SS} . Combining a nonlinear PID with friction compensation, the system's performance will excel in both steady state and transient response analysis.

3 RESULTS AND DISCUSSION

3.1 Simulation Analysis

A step input is given to the compensated system. For the first simulation, a value of 1, equivalent to 1 volt, is set as reference input. Figure 17 shows the transient response and the steady-state phase of all the compensators analyzed. Figure 18 presents a closeup of the transient response from Fig. 14. The steady-state performance of the controllers is tabulated in Table 6, and the transient response performance is tabulated in Table 7.

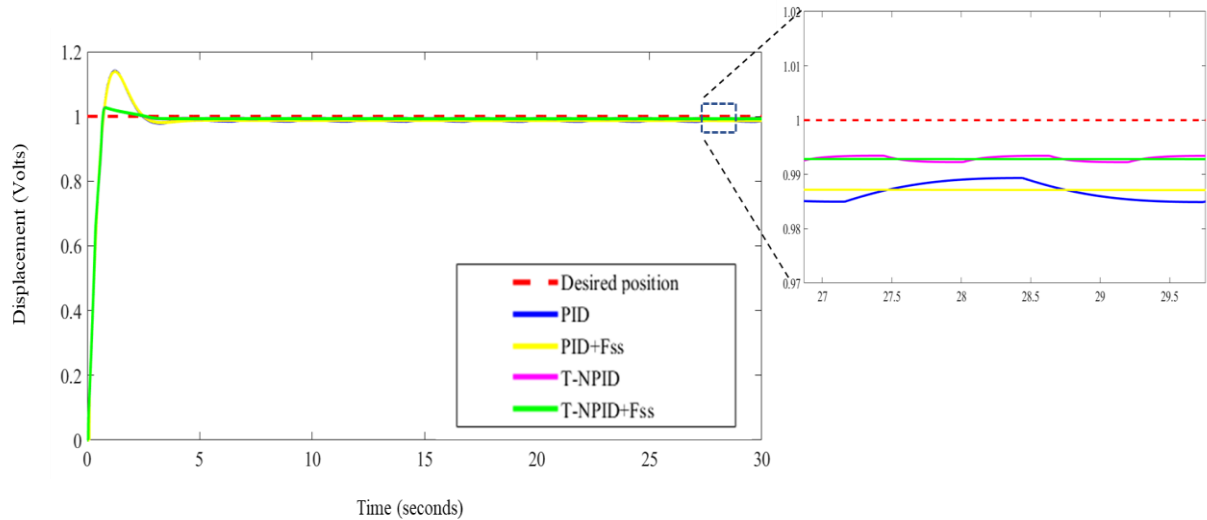


Fig. 17: Simulation of system response of all controllers.

Table 6: Simulation results of the steady-state performance comparison

Steady-state parameter	PID	PID+ F_{SS}	T-NPID	T-NPID+ F_{SS}
Desired output (volts)	1	1	1	1
Actual output (volts)	0.987	0.987	0.993	0.993
Steady-state error, SSE (volts)	0.013	0.013	0.007	0.007
% Steady-state error, %SSE (%)	1.3	1.3	0.7	0.7

For the data tabulated in Table 6, the T-NPID without and with the F_{SS} presents better steady performance than base PID controllers. Although the value of the actual output of the controllers with friction compensators compared to the controllers without the friction compensators is the same, the close-up of the steady-state condition shows that the controllers with the friction compensators can compensate for the small oscillation due to the estimated friction. This oscillation due to friction is also known as the position-hunting phenomenon [33].

As tabulated in Table 7, the transient response data presents no significant compromise due to the integration of F_{SS} to both PID and T-NPID. T-NPID shows a significant improvement of the transient responses over the classical PID, especially to the Maximum overshoot, C_{MAX} , corresponding to the reduction and improvement of Percent overshoot, % OS. The results parallel with the nonlinear PID controller's response as presented by Salim et al. [22] and Jamian et al. [23], where the overshoot is drastically reduced.

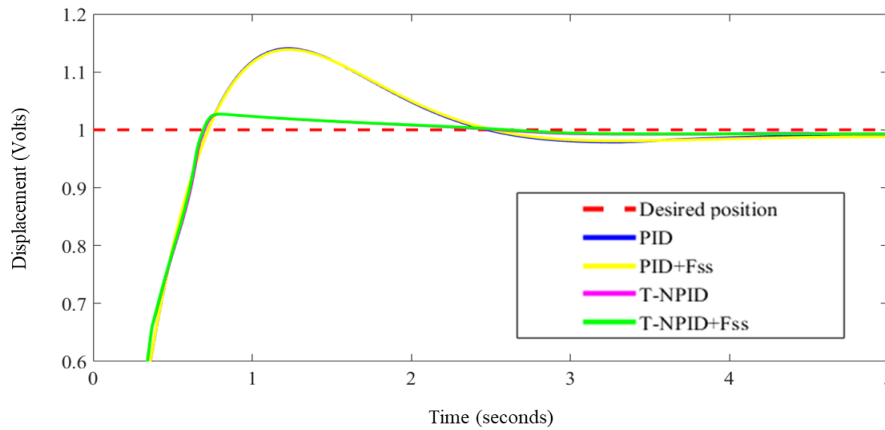


Fig. 18: The close-up transient response of each controller in simulation.

Table 7: Simulation results of the transient response performance comparison

Transient response parameter	PID	PID+F _{SS}	T-NPID	T-NPID+F _{SS}
Rise time, T _R (seconds)	0.49	0.49	0.53	0.53
Percent overshoot, %OS (%)	14.00	13.90	2.7	2.7
Maximum overshoot, C _{MAX} (volts)	1.140	1.139	1.027	1.027
Peak time, T _P (seconds)	1.23	1.23	0.8	0.8
Settling time, T _S (seconds)	2.35	2.36	1.621	1.653

3.2 Experimental Analysis

In the experimental analysis, the input given to the system is 100 mm, compared to 1 volt in the simulation analysis. For the Enfield actuator and encoder, a 1-volt conversion to mm is 30.48 mm (1 inch) of displacement, as mentioned in the product specification sheet. A displacement of 100 mm is given as the input rather than 30.48 mm as the unit is significantly presentable. Figure 19 presents the overall transient and steady-state response for all the controllers. Figure 20 shows a closeup of the controller's transient response. The data obtained is noticeably "noisy" compared to the simulation figures due to encoders or position sensors. Visually observed, the PID controller performs the least during transient response as the overshoot is the highest. Other controllers can control and reduce the overshoot during transient response. Besides PID, other controllers were also able to maintain the final position at the steady state, as the closeup Fig. 20 shows. PID controller offsets significantly at the steady state compared to other controllers.

Table 8 tabulates the steady-state performance of the controllers. T-NPID+F_{SS} presents the best performance of precise positioning at 0.3% SSE. A slight increase in the steady-state error is seen for the T-NPID. In the author's view, this is on par with T-NPID+F_{SS}. The small performance gain from T-NPID of 0.74% SSE to 0.30% is partially due to the noise measurement in the error sensor, especially at the time of steady-state ($t=50$ seconds). An additional performance measure, such as the IAE index performance, will present a complete conclusion of the controller's performance as all transient response, steady-state, and position hunting effect is calculated at once. The PID+F_{SS} controller alone can increase the precise positioning performance of the controller (from 2.60% SSE to 1.04% SSE). Figure 20 shows the close-up transient response performance of each controller. PID controller presents the highest overshoot, which means the controller performs the least.

PID+ F_{SS} is not expected to improve the transient response as observed during simulation; however, in the experimental stage, PID+ F_{SS} is able to slightly improve on the transient response, bringing the performance closer to T-NPID and T-NPID+ F_{SS} . The transient response performance is tabulated in Table 9.

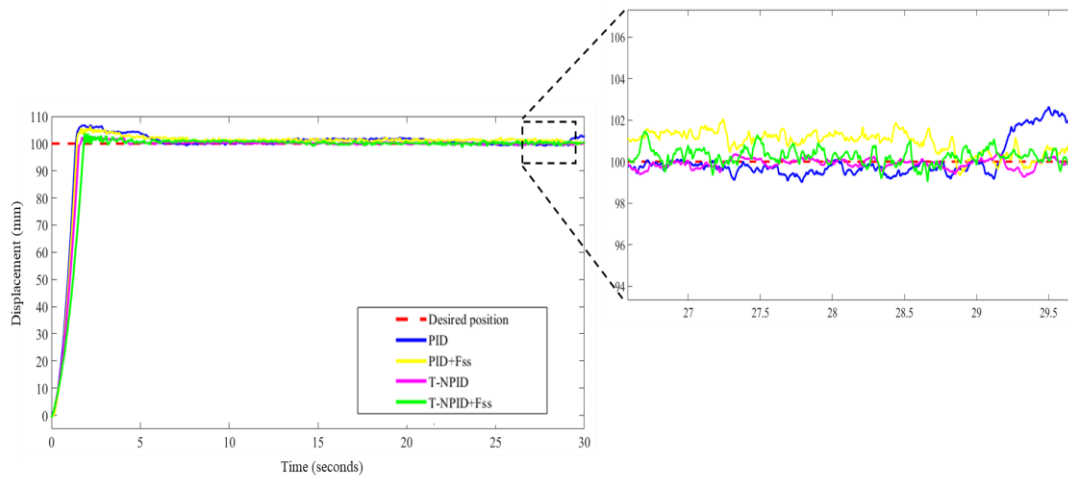


Fig. 19: Experimental of system response of all controllers.

Table 8: Experimental results of the steady-state performance comparison

Steady-state parameter	PID	PID+ F_{SS}	T-NPID	T-NPID+ F_{SS}
Desired output (mm)	100	100	100	100
Actual output (mm)	102.60	98.96	99.26	100.30
Steady-state error, SSE (mm)	2.60	1.04	0.74	0.30
% Steady-state error, %SSE (%)	2.60	1.04	0.74	0.30

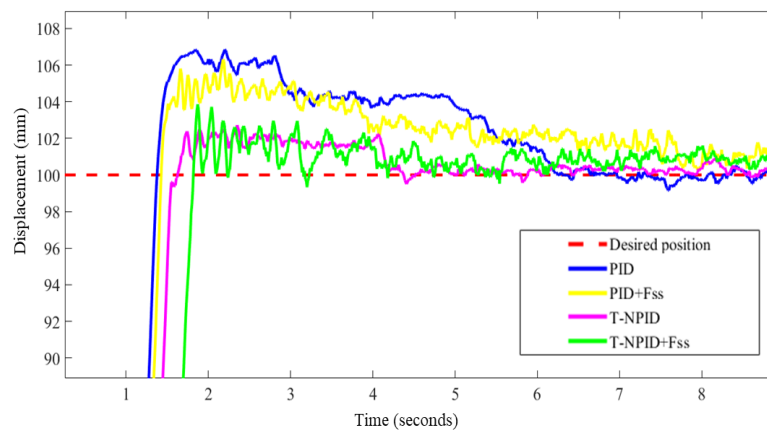


Fig. 20: Transient response experimental.

Figure 21 shows the single response of the PID controller. There is a noticeable position hunting at the desired position line. The phenomenon is in line with the previous research that internal friction will manage to cause the effect of position hunting in a system.

Figure 22 shows the PID+ F_{SS} . The noticeable position hunting has been minimized. This improvement is validated by the measurement of IAE, where a significant reduction in the IAE for PID+ F_{SS} compared to PID as tabulated in Table 10. The improvement is from 128 (volt²) to 113.7 (volt²), a reduction of 11.17%.

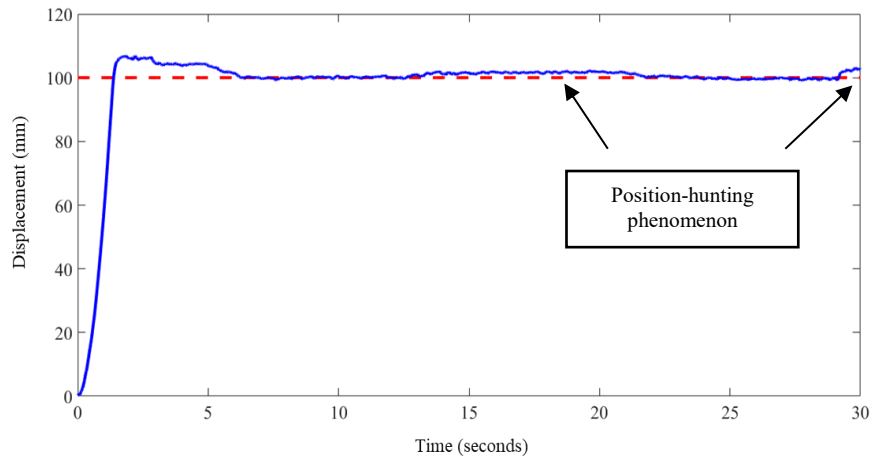


Fig. 21: The PID controller response.

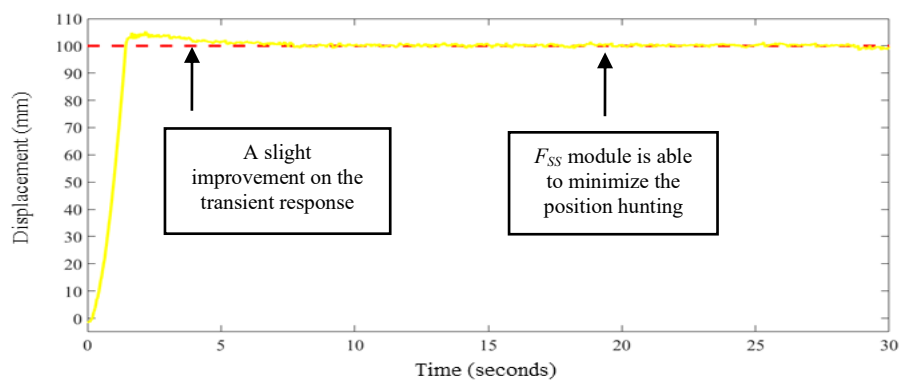


Fig. 22: The PID+F_{SS} controller response.

Figure 23 shows the T-NPID+F_{SS} system response. The controller and module can maintain the precise positioning performance and reduce the overshoot, reflecting improvement in the transient response.

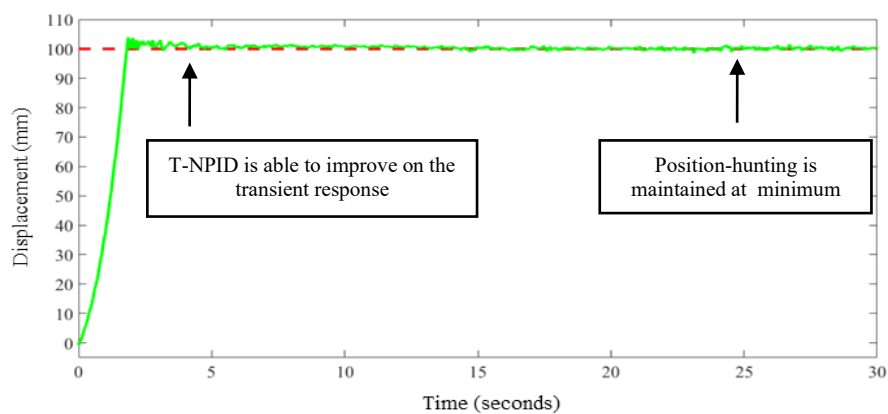


Fig. 23: The T-NPID+F_{SS} controller response.

Most previous research in the literature focuses on friction compensation to sinusoidal tracking performance. The closest to a step response analysis is a multi-steps positioning tracking performance by Rahman et al. [21]. The author analyzed both sinewave trajectories and multi-steps polynomial trajectory. The multi-steps reference input is trapezoidal shapes

multi-steps, as shown in Fig. 24. Therefore, the performance measures were RMSE and mean steady-state errors (SSE). Transient response analyses were not presented. However, the comparison of controllers with and without the LuGre friction compensator was presented, where the proposed DAB-SMC controller improved by 1.77 mm in mean SSE with the friction observer active (in terms of percentage improvement, the numbers were unclear). The performance of controllers without friction observer is shown in Fig. 25. The SSE results without the observer are visible.

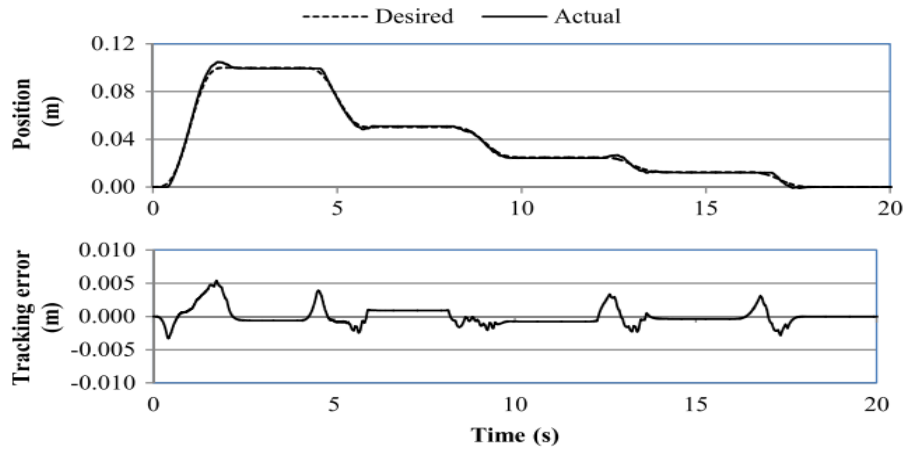


Fig. 24: Multi-steps trajectory performance analysis for DAB-SMC with LuGre friction observer [21].

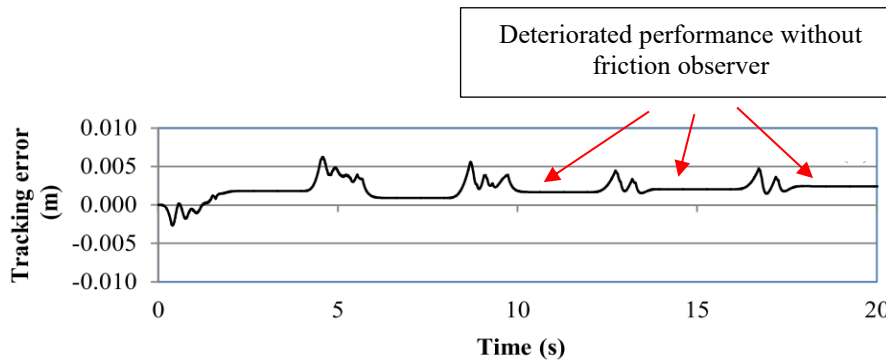


Fig. 25: Tracking error for DAB-SMC without friction observer [21].

Table 9: Experimental results of the transient response performance comparison

Transient response parameter	PID	PID+ F_{SS}	T-NPID	T-NPID+ F_{SS}
Rise time, T_R (seconds)	0.895	0.943	1.068	1.171
Percent overshoot, %OS (%)	6.80	4.9	2.70	3.30
Maximum overshoot, C_{MAX} (mm)	106.8	104.9	102.7	103.3
Peak time, T_P (seconds)	1.84	2.18	2.35	1.58
Settling time, T_S (seconds)	5.573	5.215	2.377	3.253

Table 9 tabulates the transient response of each controller. The controller with F_{SS} , PID+ F_{SS} , and T-NPID+ F_{SS} does not necessarily improve overshoot, respectively, as shown for the T-NPID+ F_{SS} controller. PID+ F_{SS} is observed to slightly improve on the overshoot (from 6.8% to 4.9%, an improvement of 1.9%), whereas for T-NPID, the overshoot slightly increases (from 2.7 % to 3.3%). The 0.6% decrease is again due to the noise of the sensor signal. As shown in Fig. 26, comparing T-NPID and T-NPID+ F_{SS} , the overshoots are

comparably on par. There is a slight suppression during overshoot for T-NPID+ F_{SS} due to the friction module compensating. The settling time, T_s , for both T-NPIDs is significantly improved over PID by around 40 to 60%.

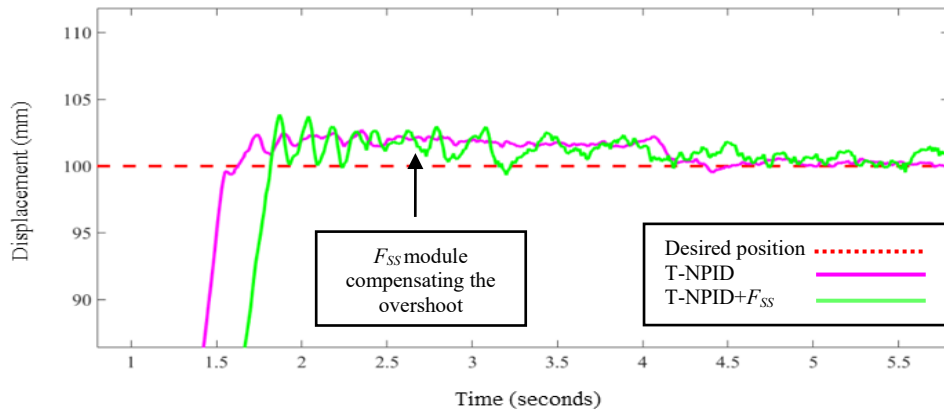


Fig. 26: The T-NPID and T-NPID+ F_{SS} overshoot comparison.

Table 10 tabulates the IAE performance index of each controller in the experimental condition based on Eq. (18). The IAE for each component of the compensator adds improvement. PID+ F_{SS} reduces the IAE from 128 to 113.7 (mm). The final T-NPID+ F_{SS} controller produces the least IAE, which shows this controller produces the best transient response and the steady-state position. Figure 27 shows the IAE performance index in graphical form.

$$IAE = \int_0^{\infty} |r(t) - y(t)| dt \quad (18)$$

where $r(t)$ and $y(t)$ are desired and actual positions, respectively.

Table 10: IAE performance comparison

Performance measure	PID	PID+ F_{SS}	T-NPID	T-NPID+ F_{SS}
IAE (mm)	128	113.7	108.2	104.9

Table 11 tabulates the percentage of increased performance of important parameters in steady-state and transient response, compared to the base PID controller. The percentage of improvement of the parameters is calculated based on Eq. (19) [41]. A higher percentage denotes a better improvement of the parameter.

$$\text{Percent Improved Value Reduction} = \left[\frac{\text{Improved value} - \text{Benchmark value}}{\text{Benchmark value}} \right] \times 100\% \quad (19)$$

Table 11: Percentage of reduction of parameter performance of each controller

Performance parameter	PID+ F_{SS} with PID	T-NPID with PID	T-NPID+ F_{SS} with PID
Steady-state error, SSE (%)	60	70.77	88.46
IAE (%)	11.17	15.47	18.05
Percent overshoot, %OS (%)	29.94	60.29	51.47
Settling time, T_s (%)	6.42	57.35	41.63

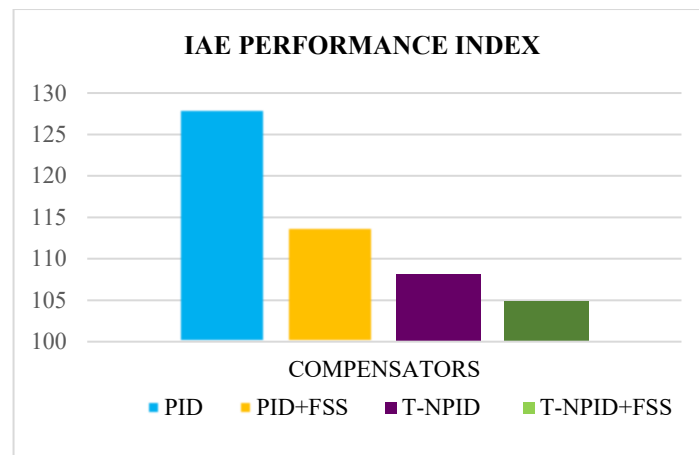


Fig. 27: IAE performance comparison experimental.

SSE recorded the best improvement among the parameters measured by the T-NPID+F_{SS} at 88.46% improvement. The performance follows T-NPID (70.77%) and PID+F_{SS} (60%). PID+F_{SS} alone is respectable as a high percentage of improvement is seen by integrating the F_{SS} module. IAE index performance also presents an improvement of 18.05% by the final controller, overcoming the other controllers. The transient response, such as %OS and T_s, T-NPID, slightly overcomes the T-NPID+F_{SS}. As explained in the previous discussion, this is highly due to the noise in the measurement sensor during measurement (point-to-point measurement), but the performance is on-par. Visually analyzed, these two transient response parameters are on par for T-NPID and T-NPID+F_{SS}. IAE validates that overall performance as TNPID+F_{SS} produced the least error and therefore is the best controller in this case.

Comparing the analysis to the previous research, as stated earlier, the included literature primarily analyzes sinewave tracking trajectories with different amplitudes and frequencies. In this research, step positioning performance is analyzed. Friction compensation is also significant in step positioning on top of trajectories. As presented by Soleymani et al. [19], Tran et al. [20], and Rahman et al. [21], the RMSE errors for sinewave tracking were reduced from 15% to up to 50%. Figure 28 shows the tracking error of a sinewave trajectory comparison between two different friction models applied where GMS model performs better than Stribeck model. This research and the previous literature prove that friction compensation is highly important and is able to add performance to any primary controller. Even though the static friction model is relatively simple compared to the dynamic models, the model is significant to achieve better precise positioning of the system.

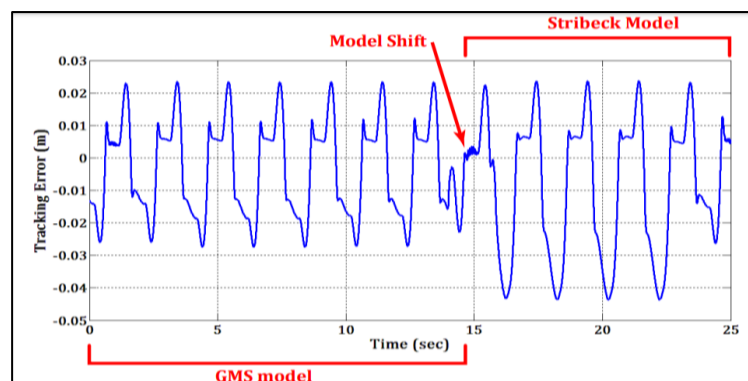


Fig. 28: Tracking error analysis performed by Soleymani et al. [19].

4. CONCLUSION

A proposed static friction compensator module has been designed, applied to several proposed controllers, and analyzed to achieve the best actual position versus the desired position for a pneumatic actuator. The friction was successfully identified, modeled, and compensated by applying the static friction model. Combining the static friction model compensation with the T-NPID, T-NPID+ F_{SS} has been proven to obtain an exceptional precise positioning for the pneumatic system. The precise positioning performance has been improved by 88.46% to the reference controller. A sinewave tracking performance will also need to be analyzed, as this analysis will conclude the performance of this research to the previous related research. A tracking differentiator algorithm is desirable to be integrated into a feedforward configuration and has been proven to improve servo pneumatic trajectory performance [42]. Further enhancing this research, the friction model can be identified by adopting AI optimization tools, such as Genetic Algorithm (GA) and Neural Networks (NN) [43-44]. By adopting the tools, the model's accuracy in predicting actual friction is also improved. A higher accuracy friction model will be able to cater to better friction compensation, resulting in a higher precise positioning system.

ACKNOWLEDGMENT

The authors would like to acknowledge the financial support by the Ministry of Higher Education (MOHE) of Malaysia through the Fundamental Research Grant Scheme (FRGS), No: FRGS/1/2020/TK0/UTEM/02/33 and Universiti Teknikal Malaysia Melaka (UTeM) with reference number FRGS/1/2020/FKP-COSSID/F00444.

REFERENCES

- [1] Hildebrandt A, Neumann R, Sawodny O. (2010) Optimal system design of SISO-servopneumatic positioning drives. *IEEE Transaction on Control Systems Technology*, 18(1): 35-44.
- [2] Noor SBM, Ali HI, Marhaban MH. (2011) Design of combined robust controller for a pneumatic servo actuator system with uncertainty. *Scientific Research and Essays*, 6(4): 949-965 3.
- [3] Lu CH, Hwang YR. (2012) A model reference robust multiplesurfaces design for tracking control of radial pneumatic motion systems. *Nonlinear Dynamics*, 67(4): 2585-2597.
- [4] Salim SN, Rahmat MF, Faudzi AAM, Ismail ZH, Sunar N. (2014) Position control of pneumatic actuator using self-regulation nonlinear PID. *Mathematical Problems in Engineering*, 2014.
- [5] Beater P. (2007) *Pneumatic Drives*. Springer-Verlag Berlin Heidelberg.
- [6] Faisal WT, Albagul A. (2004) Anti-windup scheme for practical control of positioning systems. *IIUM Engineering Journal*, 5(2): 1-15.
- [7] Andrighetto PL, Valdiero AC, Carlotto L. (2006) Study of the friction behavior in industrial pneumatic actuators. In *ABCM Symposium series in mechatronics*, 2: 369-376.
- [8] Saravanakumar D, Mohan B, Muthuramalingam T. (2017) A review on recent research trends in servo pneumatic positioning systems. *Precision Engineering*, 49 :481-492.
- [9] Johnson MA, Moradi MH. (2005) *PID control*. London, UK, Springer-Verlag London Limited.
- [10] Vinagre BM, Monje CA, Calderón AJ, Suárez JI. (2007) Fractional PID controllers for industry application. A brief introduction. *Journal of Vibration and Control*, 13(9-10): 1419-1429.
- [11] Zainal A, Wahab NA, Yusof MI. (2023) PLC-based PID controller for real-time pH neutralization process using Palm Oil Mill Effluent. *IIUM Engineering Journal*, 24(1): 244-255.

- [12] Priyanka EB, Maheswari C, Ponnibala M, Thangavel S. (2019) SCADA based remote monitoring and control of pressure & flow in fluid transport system using IMC-PID controller. *Advances in Systems Science and Applications*, 19(3): 140-162.
- [13] Ashmi M, Anila M, Sivanandan KS. (2021) Comparison of SMC and PID controllers for pneumatically powered knee orthosis. *Journal of Control, Automation and Electrical Systems*, 32(5): 1153-1163.
- [14] Jouppila VT, Gadsden SA, Bone GM, Ellman AU, Habibi SR. (2014) Sliding mode control of a pneumatic muscle actuator system with a PWM strategy. *International Journal of Fluid Power*, 15(1): 19-31.
- [15] Richer E, Hurmuzlu Y. (2000) A high performance pneumatic force actuator system: part II nonlinear controller design. *Journal of Dynamic Systems, Measurement and Control*, 122(3): 426-34.
- [16] Zhu Y, Barth EJ. (2010) Accurate sub-millimeter servo-pneumatic tracking using model reference adaptive control (MRAC). *International Journal of Fluid Power*, 11(2): 43-55.
- [17] Takosoglu JE, Laski PA, Blasiak S. (2012) A fuzzy logic controller for the positioning control of an electro-pneumatic servo-drive. *Proceedings of the Institution of Mechanical Engineers, Part I: Journal of Systems and Control Engineering*, 226(10): 1335-1343.
- [18] Ren HP, Jiao SS, Wang X, Li J. (2020) Adaptive RBF Neural Network Control Method for Pneumatic Position Servo System. *IFAC-PapersOnLine*, 53(2): 8826-8831.
- [19] Soleymani F, Rezaei SM, Sharifi S, Zareinejad M. (2016) Position control of a servo-pneumatic actuator using generalized Maxwell-Slip friction model. In 2016 4th International Conference on Robotics and Mechatronics (ICROM): 26 Oct 2016; Edited by IEEE, pp 246-251.
- [20] Tran XB, Nguyen VL, Nguyen NC, Pham DT, Phan VL. (2019) Sliding mode control for a pneumatic servo system with friction compensation. In *Advances in Engineering Research and Application: Proceedings of the International Conference on Engineering Research and Applications, ICERA 2019*: 1 Dec 2019; Edited by Springer International Publishing, pp 648-656.
- [21] Rahman RA, He L, Sepehri N. (2016) Design and experimental study of a dynamical adaptive backstepping-sliding mode control scheme for position tracking and regulating of a low-cost pneumatic cylinder. *International Journal of Robust and Nonlinear Control*, 26(4): 853-875.
- [22] Salim SN, Amran AC, Faudzi AAM, Ismail ZH, Rahmat MF, Sunar NH, Shamsudin SA. (2015). A study on tracking performance of the pneumatic system with enhanced NPID controller. In 2015 10th Asian control conference (ASCC): 31 May 2015; Edited by IEEE, pp 1-6.
- [23] Jamian S, Salim SN, Junoh SCK, Kamarudin MN, Abdullah L. (2020) Nonlinear Proportional Integral (NPI) Double Hyperbolic Controller for Pneumatic Actuator System. In *Advances in Electronics Engineering: Proceedings of the ICCEE 2019*: 29-30 April 2019; Kuala Lumpur, Malaysia. Edited by Springer Singapore, pp 221-229.
- [24] Junoh SCK, Salim SN, Abdullah L, Anang NA, Chiew TH, Retas Z. (2017) Nonlinear PID triple hyperbolic controller design for XY table ball-screw drive system. *International Journal of Mechanical and Mechatronics Engineering*, 17(3): 1-10.
- [25] Kamaludin KN, Abdullah L, Salim SN, Jamaludin Z, Maslan MN, Rahmat MF. (2022) Comparison of a Double and Triple Nonlinear Hyperbolic Proportional-Integral-Derivative (PID) compensator for a servo pneumatic actuator. In 2022 13th Asian Control Conference (ASCC): 4 May 2022; Jeju, Korea, Edited by IEEE, pp 1775-1781.
- [26] Abdullah L, Jamaludin Z, Chiew TH, Rafan NA, Mohamed MS. (2012) System identification of XY table ballscrew drive using parametric and non parametric frequency domain estimation via deterministic approach. *Procedia Engineering*. 41: 567-574.
- [27] Dermawan D, Abbas H, Syam R, Djafar Z, and Muhammad AK. (2020) Dynamic modeling of a single-link flexible manipulator robot with translational and rotational motions. *IIUM Engineering Journal*. 21(1): 228-239.
- [28] Rahmat MF, Sunar NH, Salim SN, Abidin MS, Fauzi AM, Ismail ZH. (2011) Review on modeling and controller design in pneumatic actuator control system. *International Journal on Smart Sensing and Intelligent Systems*. 4(4): 630-661.

- [29] Jamian S, Salim SN, Kamarudin MN, Abdullah L, Hanafiah MA. (2018) Modeling of a single rod double acting pneumatic actuator system. In Proceedings of Symposium on Electrical, Mechatronics and Applied Science (SEMA ,18): 8 December 2018; Melaka, Malaysia. pp 45-46.
- [30] Ljung L. (1995) System Identification Toolbox: User's Guide. Natick, MA, USA: MathWorks Incorporated.
- [31] Sulaiman SF, Rahmat MF, Faudzi AA, Osman K. (2016) Linear and nonlinear ARX model for intelligent pneumatic actuator systems. *Jurnal Teknologi*. 78(6): 21-28.
- [32] Chiew TH, Jamaludin Z, Hashim AB, Rafan NA, Abdullah L. (2013) Identification of friction models for precise positioning system in machine tools. *Procedia Engineering*. 53: 569-578.
- [33] De Wit CC, Olsson H, Astrom KJ, Lischinsky P. (1995) A new model for control of systems with friction. *IEEE Transactions on automatic control*. 40(3): 419-425.
- [34] Meng D, Tao G, Chen J, Ban W. (2011) Modeling of a pneumatic system for high-accuracy position control. In Proceedings of 2011 International Conference on Fluid Power and Mechatronics: 17-20 August 2011; Beijing, China. pp 505-510.
- [35] Salim SN. (2014) Modeling and Control Design of an Industrial Pneumatic Actuator System. PhD thesis, Universiti Teknologi Malaysia.
- [36] Junoh SCK. (2019) NPID Double Hyperbolic Controller for Improving Tracking Performance of XY Table Ballscrew Drive System. MSc thesis, Universiti Teknikal Malaysia Melaka.
- [37] Jamaludin Z. (2008) Disturbance Compensation for Machine Tools with Linear Motors. PhD thesis. Ketholieke Universiteit Leuven, Belgium.
- [38] Seraji H. (1997) A new class of nonlinear PID controllers. In IFAC Proceedings Volumes 30.20: 1 September 1997; pp 65-71.
- [39] Albatran S, Alatoum A, Al Khalailah AR. (2021) Informative Order-Reduction of Underdamped Third-Order Systems. *IEEE Access*. 9: 88512-88523.
- [40] Su YX, Sun D, Duan BY. (2005) Design of an enhanced nonlinear PID controller. *Mechatronics*. 15(8): 1005-1024.
- [41] Abdullah L. (2014) A New Control Strategy for Cutting Force Disturbance Compensation for XY Table Ball Screw Driven System. PhD thesis. Universiti Teknikal Malaysia Melaka.
- [42] Zhao L, Xia Y, Yang Y, Liu Z. (2017) Multi controller positioning strategy for a pneumatic servo system via pressure feedback. *IEEE Transactions on Industrial Electronics*. 64(6): 4800-4809.
- [43] Carducci G, Giannoccaro NI, Messina A, Rollo G. (2006) Identification of viscous friction coefficients for a pneumatic system model using optimization methods. *Mathematics and Computers in Simulation*. 71(4-6): 385-94.
- [44] Wang J, Wang JD, Daw N, Wu QH. (2004) Identification of pneumatic cylinder friction parameters using genetic algorithms. *IEEE/ASME transactions on mechatronics*. 9(1): 100-107.